ACS APPLIED MATERIALS & INTERFACES

Research Article

Cite This: ACS Appl. Mater. Interfaces 2018, 10, 7079−7086

www.acsami.org

High-Index Faceted Porous Co_3O_4 Nanosheets with Oxygen Vacancies for Highly Efficient Water Oxidation

Renjie Wei,[†,‡,§] Ming Fang,[†,§] Guofa Dong,[†] Changyong Lan,[†,‡,§] Lei Shu,[†,§] Heng Zhang,[†,‡] Xiuming Bu,[†,‡] and Johnny C. Ho*[,†,‡,§]

[†]Department of Materials Science and Engineering and [‡]State Key Laboratory of Millimeter Waves, City University of Hong Kong, Kowloon, Hong Kong

[§]Shenzhen Research Institute, City University of Hong Kong, Shenzhen 518057, P. R. China

Supporting Information

ABSTRACT: Because of sluggish kinetics of the oxygen evolution reaction (OER), designing low-cost, highly active, and stable electrocatalysts for OER is important for the development of sustainable electrochemical water splitting. Here, {112} high-index facet exposed porous Co_3O_4 nanosheets with oxygen vacancies on the surface have been successfully synthesized via a simple hydrothermal method followed by $NaBH_4$ reduction. As compared with the pristine and other faceted porous Co_3O_4 nanosheets (e.g., {110} and {111}), the as-prepared {112} faceted porous nanosheets exhibit a much lower overpotential of 318 mV at a current density of 10 mA cm^{-2}. Importantly, these nanosheets also give excellent electrochemical stability, displaying an insignificant change in the required overpotential at a current density of 10 mA cm^{-2} even after a 14 h long-term chronoamperometric test. All these superior OER activity and stability could be attributed to their unique hierarchical structures assembled by ultrathin porous nanosheets, {112} high-index exposed facets with higher ratio of Co^{2+}/Co^{3+} and oxygen vacancies on the surface, which can substantially enhance the charge transfer rate and increase the number of active sites. All these findings not only demonstrate the potency of our Co_3O_4 nanosheets for efficient water oxidation but also provide further insights into developing cost-effective and high-performance catalysts for electrochemical applications.

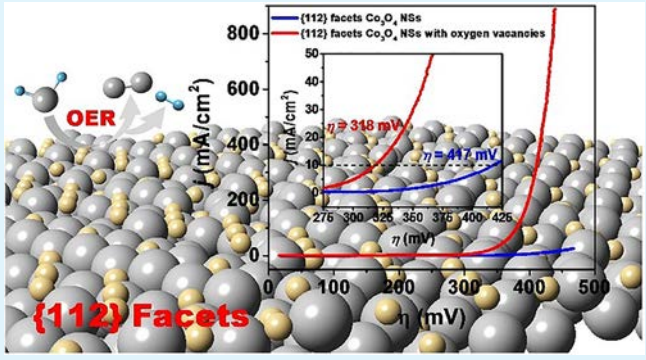

KEYWORDS: *cobalt oxide, high-index facets, oxygen vacancy, oxygen evolution reaction*

1. INTRODUCTION

Because of its high specific energy content and carbon neutral combustion products, hydrogen has been long considered as an alternative fuel for meeting the increased global energy consumption. In this regard, among many hydrogen production methods, electrochemical water splitting with two half-reactions driven by renewable energy sources is widely explored to generate hydrogen in an environmental-friendly manner.[1−3] However, in comparison to hydrogen evolution reaction (HER), oxygen evolution reaction (OER) with a multistep, four-electron process evolved is severely constrained by its sluggish kinetics.[4] Up until now, noble-metal-based materials such as Ir oxides and Ru oxides are the typical electrocatalysts employed to lower the substantially large overpotential required for OER, in which their scarcity and associated high cost greatly hinder their practical utilizations.[5−7] As a result, developing high-performance and low-cost OER catalysts on a large scale is essential in order to achieve sustainable water splitting.

Although various kinds of Co_3O_4 materials have lately attracted extensive attention to function as promising OER catalysts, batteries, and materials for electrochemical energy conversion and storage because of their earth abundance, eco-friendliness, and cost effectiveness,[8−12] their inherently poor electrical conductivity makes them less competitive as compared with other material candidates. Many efforts have therefore been devoted to improve their conductivity as well as to increase the number of active sites. Specifically, mixing with highly conductive materials, such as metal,[13,14] carbon,[15,16] or graphene,[17−19] to form conductive composites has been commonly adopted to alleviate the conductivity issue. Besides, it has also been demonstrated that the introduction of oxygen vacancies could effectively adjust the electronic structure and greatly enhance the inherent conductivity through different complementary experimental and theoretical approaches.[20] For instance, Wang and colleagues reported a facile reduction route to prepare mesoporous Co_3O_4 nanowires with rich oxygen vacancies by $NaBH_4$ solution treatment, in which as compared with the pristine nanowires, the reduced Co_3O_4 nanowires

Received: November 30, 2017
Accepted: February 6, 2018
Published: February 6, 2018

DOI: 10.1021/acsami.7b18208
ACS Appl. Mater. Interfaces 2018, 10, 7079−7086

exhibit a considerable performance enhancement in OER process.[21] Later, Xu et al. adopted a plasma-assisted technique to generate oxygen vacancies on the surface of Co_3O_4 nanosheets via the doping of nitrogen.[22,23] Importantly, an impressively low overpotential of ca. 310 mV is only needed to obtain a current density of 10 mA cm^{-2} in their studies. On the other hand, synthesizing novel structures with more catalytically favorable surfaces is generally utilized to provide more active sites for water splitting. In particular, Stoerzinger et al. have experimentally compiled the intrinsic OER activities of IrO_2 and RuO_2 with different surface crystal orientations, supported by comprehensive simulation studies. They found that the (100)-oriented exposed facets are more electrochemically active than the thermodynamically stable (110) surfaces.[24] At the same time, Feng and co-workers have successfully prepared the {210} high-index faceted Ni_3S_2 nanosheet arrays, yielding much higher HER and OER activities and stabilities than those of the {001} low-index faceted counterparts.[25] Similarly, Liu et al. systematically studied the crystal plane effect of Co_3O_4 on overall water splitting and concluded that {111} facets exposed nanooctahedrons show the best performance.[26] These enhanced performances could be mostly attributed to the synergistic effect between nanosheet arrayed architectures and high-index facets. With the above considerations in minds, if the Co_3O_4 nanosheets can be readily fabricated with the high-index exposed facets, high porosity, and significant oxygen vacancies, the correspondingly enhanced conductivity and catalytic surface area would then contribute to the superior electrochemical activity as high-performance OER catalysts.

In this work, we demonstrate the facile fabrication of {112} high-index faceted porous Co_3O_4 nanosheets with oxygen vacancy on the surface. As expected, the synthesized electrocatalysts exhibit an excellent OER activity with a comparably low overpotential of 318 mV to reach a current density of 10 mA cm^{-2}. With an overpotential of 436 mV, the current density can be reached up to as high as 800 mA cm^{-2}. The catalyst as well shows the remarkable stability without any obvious decay of the overpotential observed after a 14 h long-term chronoamperometric test at a current density of 10 mA cm^{-2}. All these results reveal the exceptional performance and stability of our high-index faceted porous Co_3O_4 nanosheets, being one of the best OER catalysts among all Co_3O_4-based materials, evidently illustrating their promising potency for high-performance electrochemical applications.

2. EXPERIMENTAL SECTION

Preparation of {112} Faceted Porous Co_3O_4-B Nanosheets. All chemicals were purchased in the analytical grade and were used without any further purification. In a typical preparation,[27] 1.26 g of $Co(NO_3)_2{\cdot}6H_2O$ was dissolved in 14 mL of methanol. Once $Co(NO_3)_2{\cdot}6H_2O$ got dissolved completely, 0.2 mL of benzyl alcohol was added into the mixture. After stirring for another 1 h, the solution was transferred into a Teflon-lined stainless steel autoclave (25 mL in volume), which was subsequently heated to 180 °C and maintained at that temperature for 24 h. Then, it was cooled to room temperature naturally. The precipitates were collected, washed with anhydrous ethanol and deionized water three times, and dried at 60 °C overnight (8 h). A lilac powder was obtained and subsequently calcined in the air with a ramp rate of 5 °C min^{-1} to 400 °C with a duration of 4 h. These intermediate products were labeled as Co_3O_4. After the thermal treatment, 30 mg of the samples (i.e., Co_3O_4) was added into 5 mL of 0.5 M $NaBH_4$ solution and immersed for 1 h. Finally, the products were filtered, washed, and dried as described above, which were labeled as Co_3O_4-B.

Characterization. The purity and crystalline structure of the samples were next evaluated by powder X-ray diffraction (XRD) employing a scanning rate of 0.05°/s in a 2θ scan range from 10° to 80°, using a Bruker D2 Phaser (Bruker, Billerica, MA) instrument equipped with monochromatized Cu Kα radiation. The morphologies and dimensions of the samples were observed by scanning electron microscopy (SEM, Phenom Pro, Phenom-World, The Netherlands) with an accelerating voltage of 10 kV and field-emission SEM (SU-8010, Hitachi, Tokyo, Japan) with an accelerating voltage of 15 kV. Transmission electron microscopy (TEM) and high-resolution (HR) TEM were conducted by a Tecnai G^2 F30 (FEI, Hillsboro, OR) using an accelerating voltage of 200 kV. Brunauer–Emmett–Teller (BET) specific surface areas of the samples were assessed on the basis of nitrogen adsorption isotherms using a NOVA 1200e gas adsorption apparatus (Quantachrome Instruments, Boynton Beach, FL). X-ray photoelectron spectroscopy (XPS) was recorded on a VG Multilab 2000 (Thermo Fisher Scientific, Waltham, MA) photoelectron spectrometer using monochromatic Al Kα radiation under vacuum at a pressure of 2×10^{-6} Pa. All of the binding energies were referenced to the C 1s peak at 284.8 eV of the surface adventitious carbon.

Electrochemical Measurements. For a typical electrochemical measurement, 5 mg of electrocatalysts (as-synthesized samples) was dispersed in a mixed solution containing 100 μL of deionized (DI) water, 340 μL of ethanol, and 20 μL of Nafion (5 wt %) by sonication for 2 h to obtain a homogeneous ink. Then, 10 μL of electrocatalysts ink were drop-casted on the polished glassy carbon electrode with diameter in 5 mm and area in 0.196 cm^2, which meant that the loading amount was about 0.553 mg cm^{-2}. The fabricated electrode was dried at ambient condition overnight (8 h). All electrochemical characterizations were investigated on a Gamry 300 electrochemical workstation connected with a standard three-electrode configuration under 25 °C using a constant temperature bath. The fabricated electrode sample was used as the working electrode. A saturated calomel electrode (SCE) and a Pt wire were employed as the reference electrode and counter electrode, respectively. All potentials reported in this work were calibrated versus the reversible hydrogen electrode (RHE) using equation: $E_{RHE} = E_{SCE} + (0.2415 + 0.059 \times pH)$ V, where E_{RHE} is the potential referred to RHE and E_{SCE} is the measured potential against SCE reference electrode. The OER activity was surveyed in 1 M KOH aqueous solution (pH = 13.73) by linear sweep voltammetry (LSV) at a scan rate of 5 mV s^{-1}. To keep the electrode surface in a relatively stable state, 10 cyclic voltammetry (CV) cycles were operated before the assessment of OER activity until the redox peaks, and the oxygen evolution currents showed the unobvious change. Unless otherwise mentioned, the voltammograms were recorded with the *iR*-drop compensation automatically on the workstation. The OER stability was determined by a chronopotentiometry measurement at a current density of 10 and 50 mA cm^{-2} without any *iR*-drop compensation, accordingly. The charge-transfer resistances for different samples were determined by electrochemical impedance spectroscopy (EIS) in the frequency range between 0.01 Hz and 300 kHz at 5 mV rms.

3. RESULTS AND DISCUSSION

As shown in Supporting Information Figure S1, the crystalline phase and structure of the fabricated samples were analyzed by XRD. It is clear that all of the diffraction peaks, obtained before and after the $NaBH_4$ treatment, can be indexed to the cubic Co_3O_4 phase (JCPDS card No. 71-0816), indicating that the corresponding crystalline phase is well preserved during the $NaBH_4$ reduction process. The untreated and post-treated samples are then denoted as Co_3O_4 and Co_3O_4-B, respectively. At the same time, the morphologies of all samples are also maintained after the $NaBH_4$ treatment as depicted in the SEM images in Figure 1. Both Co_3O_4 and Co_3O_4-B samples are composed of hierarchical microspheres with the diameter of ca. 10 μm (Figure 1a,b), in which these microspheres are

DOI: 10.1021/acsami.7b18208
ACS Appl. Mater. Interfaces 2018, 10, 7079–7086

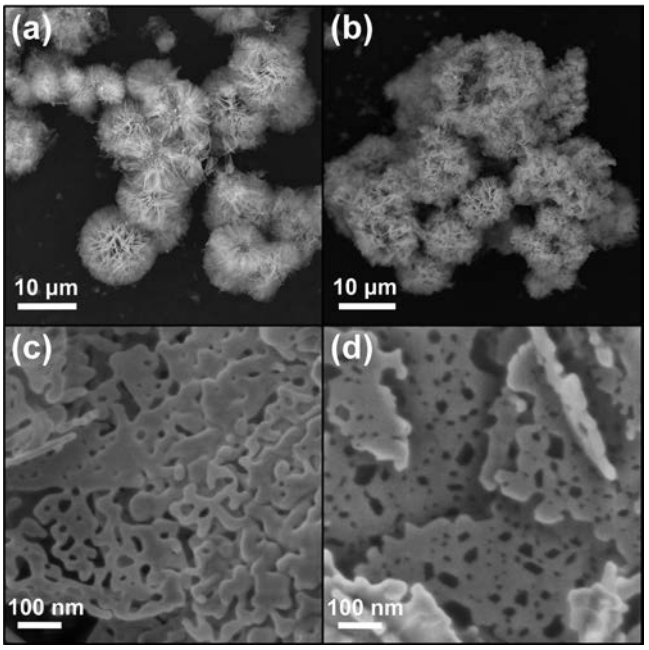

Figure 1. Representative SEM images of different Co_3O_4 nanosheets with various magnifications: (a, c) before $NaBH_4$ treatment; (b, d) after $NaBH_4$ treatment.

assembled by various amounts of nanosheets. Interestingly, there are abundant quantities of nanopores penetrating through the nanosheets (Figure 1c,d). It is worthwhile to note that these novel hierarchical nanostructures are anticipated to effectively enhance the electrolyte penetration, accelerate the bubble release rate, and avoid the random particle aggregation during the OER process.[28,29] More details regarding their morphologies were also characterized by nitrogen adsorption and desorption isotherms (Figure S2). In specific, the isotherm curves exhibit the type IV characteristic with an H3 hysteresis loop, revealing that the samples display mesoporous nanostructures and are composed of loose assemblages of sheetlike particles forming slitlike pores,[30] which is consistent with the SEM analysis discussed above. The specific surface areas of these two samples are as well calculated by the Brunauer–Emmett–Teller (BET) method, where an inconspicuous increase of the area from 44.47 to 48.01 $cm^2\ g^{-1}$ is witnessed, and negligible changes in the pore size distribution (Figure S2 inset) after $NaBH_4$ reduction further demonstrate the insignificant effect of $NaBH_4$ treatment on the morphology of Co_3O_4-B samples.

Furthermore, detailed TEM studies were also performed on the samples as displayed in Figure 2 and Figure S3. It is obvious that the sheetlike nanostructures with in-plane pores are well preserved during the $NaBH_4$ treatment, which is in the perfect agreement with the above SEM observation and BET analysis. Based on the side-view image (Figure 2b), the sheet thickness is found to be about 11 nm, indicating the ultrathin feature of the Co_3O_4-B. Since the electrocatalytic reaction usually occurs on the interface between electrocatalysts and electrolyte/intermediates, investigating the surface properties, such as surface compositions, surface defects, exposed facets, and so forth, of Co_3O_4-B nanosheets is crucial here. Explicitly, as compared with the untreated Co_3O_4 samples (Figure S3b), the surface of Co_3O_4-B nanosheets becomes rather rough since many small nanoparticles/nanoplates are formed and anchored on the surface with a typical diameter of about 4 nm (Figure 2c,d). Also, the HRTEM image of two selected representative areas (i.e., nanoplate on the surface and exposed surface) is shown in Figure 2d with the details marked by the red dotted square and circle illustrated in Figures 2e and 2f, respectively. Both display clear lattice fringes of ca. 0.28 nm, which correspond to the value of (220) planes in cubic Co_3O_4. The corresponding FFT pattern (Figure 2e, inset) and clear lattice fringe of ca. 0.24 nm (Figure 2f) further indicate that the Co_3O_4-B nanosheets also expose the same {112} high-index facet with that of untreated Co_3O_4 samples (Figure S3c). It is unique that the ultrathin

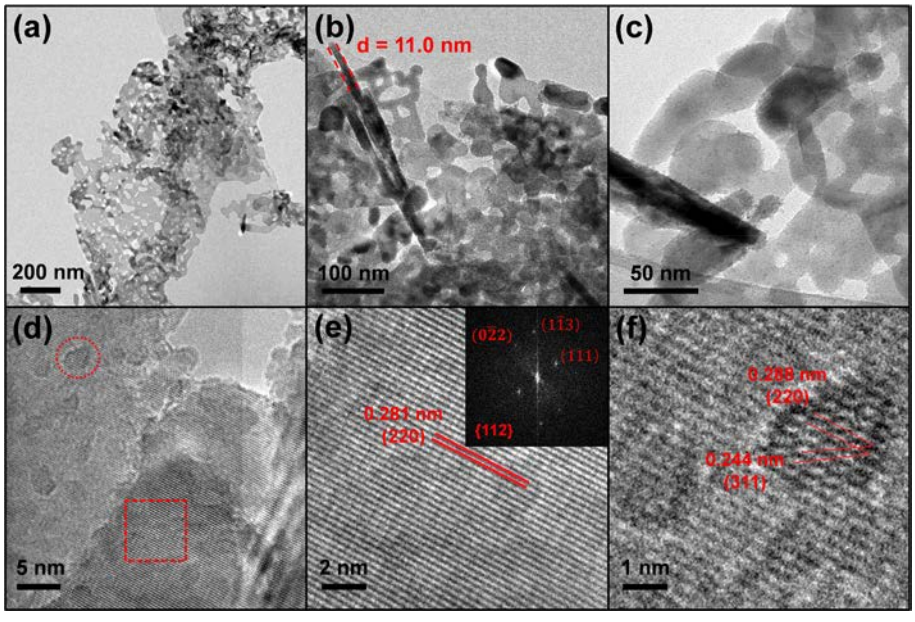

Figure 2. Typical TEM images of porous Co_3O_4-B nanosheets: (a–c) low-magnification images in vertical and parallel views; (d) high-resolution images; (e) high-magnification HRTEM image of the left red dotted square region and the corresponding FFT pattern shown in the inset; and (f) high-magnification HRTEM image of the left red dotted circle region.

DOI: 10.1021/acsami.7b18208
ACS Appl. Mater. Interfaces 2018, 10, 7079–7086

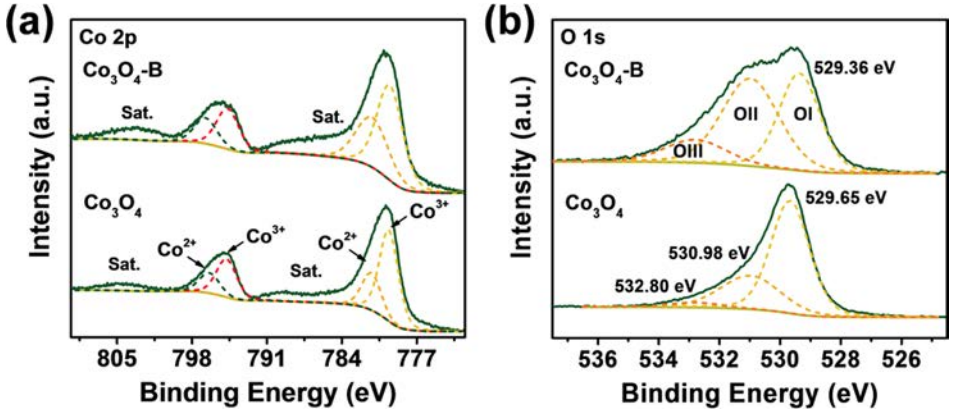

Figure 3. Comparison of XPS profiles of Co_3O_4 and Co_3O_4-B porous nanosheets: (a) high-resolution XPS Co 2p spectra and (b) the high-resolution XPS O 1s spectra.

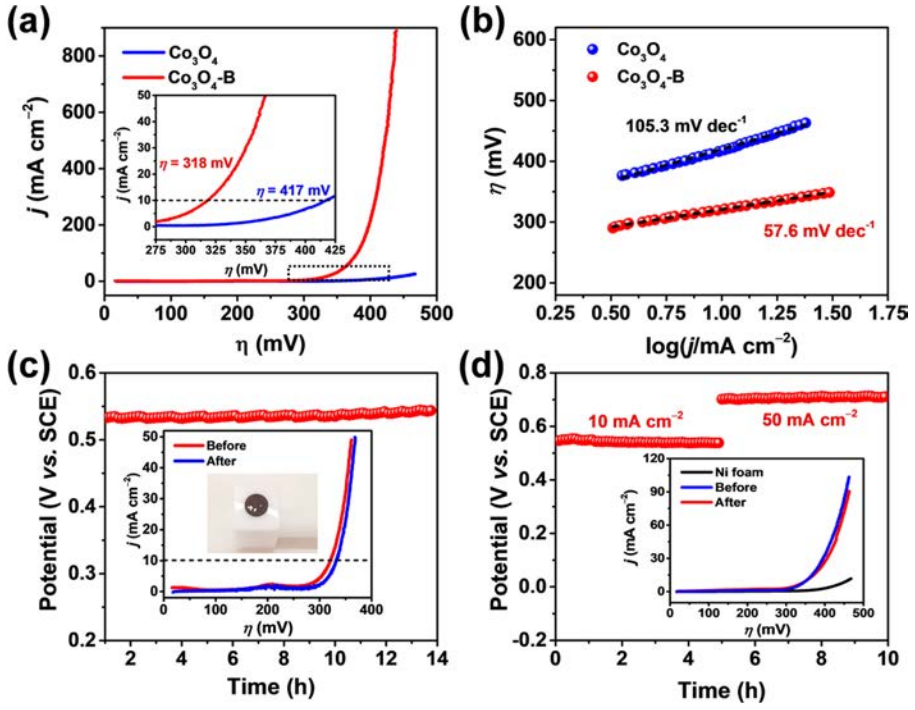

Figure 4. Electrochemical performances of different Co_3O_4 nanosheet samples. (a) Polarization curves of porous Co_3O_4 and Co_3O_4-B nanosheets with a scan rate of 5 mV s^{-1}. (b) Tafel plots of Co_3O_4 and Co_3O_4-B calculated from (a) with logarithm of current density from 0.5 to 1.5 log(j/mA cm^{-2}). (c) Long-term chronopotentiometric stability test of porous Co_3O_4-B nanosheets under a constant current density of 10 mA cm^{-2} (without an *iR* compensation); the measurement was performed on the glassy carbon electrode; inset is the polarization curves of the samples before and after chronopotentiometry. (d) Long-term chronoamperometric stability test using Ni foam as working electrode under the constant current density of 10 and 50 mA cm^{-2} for 5 h each; inset is the polarization curves of the samples before and after chronopotentiometry.

nature of these high-index faceted porous nanosheets as well as the formation of these anchored nanoparticles/nanoplates would further facilitate the catalysts to expose more edges and coordinated-unsaturated surface atoms, serving as the active sites to expedite the OER process.[31−33]

Apart from the morphology, it is also important to assess the elemental composition and corresponding chemical state of the nanosheet surface. Based on the high-resolution XPS profile of Co 2p spectra (Figure 3a), two characteristic peaks are observed at around 780.0 and 795.1 eV with a spin−orbit splitting of 15.1 eV, which can be attributed to the $2p_{3/2}$ and $2p_{1/2}$ orbitals of Co ions in Co_3O_4.[27,34] Both of them could be further deconvoluted into two separate peaks: one set locates at 779.70 and 781.35 eV for Co^{3+}, while another set locates at 794.80 and 796.45 eV for Co^{2+}.[35] As compared with the untreated Co_3O_4 nanosheets, there is an obvious increase of the integrated intensity (i.e., peak area) ratio of Co^{2+} to Co^{3+} observed for the Co_3O_4-B sample, indicating that a part of Co^{3+} ions on the nanosheet surface has been reduced to Co^{2+} ions accompanying with the generation of oxygen vacancies. Likewise, the two satellite peaks ascribed to the Co^{2+} oxidation state at the binding energy of around 785 and 803 eV are upheaved as well, further demonstrating the formation of oxygen vacancies there.[22] Moreover, Figure 3b displays the O 1s XPS profiles of both samples before and after $NaBH_4$ treatment. The fine-scanned O 1s spectra can be deconvoluted into three distinct peaks. According to the peak locations, these peaks can be identified as lattice oxygen (O_L, ca. 529.6 eV),

DOI: 10.1021/acsami.7b18208
ACS Appl. Mater. Interfaces 2018, 10, 7079−7086

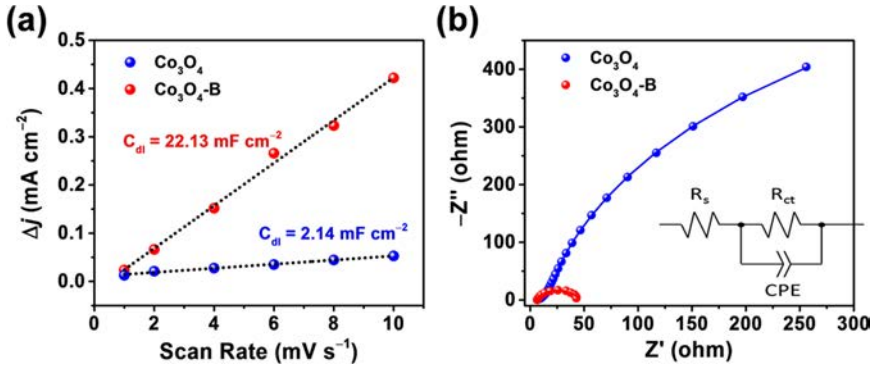

Figure 5. (a) Differences in current density variation ($\Delta j = j_a - j_c$) at a potential of 0.225 V (vs SCE) plotted against scan rate fitted to a linear regression, enabling the estimation of C_{dl}. (b) Nyquist plots obtained from the electrochemical impedance spectroscopy measurements at 1.55 V vs RHE, with a frequency range of 0.01 to 3 × 10^5 Hz.

oxygen vacancies on the surface (O_{II}, ca. 531.0 eV), and chemisorbed or dissociated oxygen or OH species on the surface (O_{III}, ca. 532.8 eV). A comparison between the Co_3O_4 and Co_3O_4-B samples shows that (1) an obvious increase in the integrated XPS intensity values (I_i) of O_{II} peak is observed, which indicates the introduction of oxygen vacancies after $NaBH_4$ reduction process, and (2) a substantial shift of O_I peak toward to the lower binding energy (ca. 529.4 eV), demonstrating that the electrons around the lattice oxygen are easily excited, which can be attributed to the reduction of Co^{3+} to Co^{2+}.[36] It is believed that the higher ratio of Co^{2+}/Co^{3+} would bestow the Co_3O_4 catalysts the better catalytic ability for OER because Co^{2+} ions are more catalytically active than Co^{3+} ions, acting as the enhanced active site for more efficient water oxidation in Co_3O_4.[22,37,38] In addition, the introduction of oxygen vacancies on the surface not only can enhance the conductivity of the catalysts but also can promote the adsorption of H_2O molecules onto the surface.[21,39] All these evidently indicate that both factors tend to play positive roles in the OER activity of Co_3O_4-B samples.

To shed light on the OER catalytic capabilities of these Co_3O_4-B nanosheets, LSV measurements were conducted using a standard three-electrode setup in 1 M KOH electrolyte (pH = 13.73) with an operating potential window from 0.2 to 0.65 V (vs E_{SCE}) at 25 °C. For comparison, Co_3O_4 nanosheets before $NaBH_4$ treatment were also performed under same test conditions. Figure 4a displays the polarization curves of these two samples after auto-*iR* compensation. Apparently, the electrochemical activity of Co_3O_4 increases significantly after the reduction process. In detail, in order to reach a current density of 10 mA cm^{-2}, a metric relevant to the solar fuel synthesis, Co_3O_4-B requires only an impressively low overpotential of 318 mV, which presents one of the best OER performances among all Co_3O_4-based materials to the best of our knowledge (Table S1). In contrast, the untreated (i.e., unreduced) porous Co_3O_4 nanosheets still need an overpotential of 417 mV to achieve the same current density. More importantly, an ultrahigh current density of 800 mA cm^{-2} can be obtained at an overpotential of as low as 436 mV for Co_3O_4-B samples, which is ca. 55-fold higher than the unreduced sample, further illustrating the superior electrochemical performance for water oxidation (see Video S1 in Supporting Information). At the same time, the Tafel slope is another important parameter used to evaluate the electrochemical kinetics of OER process, which describes the rate change of an electrochemical reaction (i.e., current density) with respect to the overpotential. Here, the logarithm of current density (log(j/mA cm^{-2})) is chosen from 0.5 to 1.5 to calculate the Tafel slope, where it shows a linear relationship with *R*-squared of ca. 99.8% and ca. 99.4% for Co_3O_4 and Co_3O_4-B samples, respectively. For the unreduced porous Co_3O_4 nanosheets, the value of Tafel slope is found to be ca. 105.3 mV dec^{-1}. After $NaBH_4$ reduction treatment, the Tafel slope value gets decreased dramatically to a much lower value of ca. 57.6 mV dec^{-1} (Figure 4b). All these point toward that the high-index faceted porous Co_3O_4-B nanosheets feature a favorable electrochemical kinetics, where only a small increase in the overpotential is required to deliver a sharp increase in the current density.

Besides, electrochemical stability is an additional critical criterion to assess the performance of electrocatalysts. In specific, the stability of porous Co_3O_4-B nanosheets configured catalysts was investigated by chronopotentiometry, in which glassy carbon were employed as the working electrode. As shown in Figure 4c, after a 14 h long-term chronoamperometric stability test, the polarization curves exhibit an insignificant change with an increase of 14 mV in the required overpotential at a current density of 10 mA cm^{-2}, demonstrating an excellent stability for the Co_3O_4-B OER catalyst. The periodic fluctuation could be ascribed to the detachment of generated oxygen bubbles on the electrode surface. Also, the decline of OER activity after chronoamperometric measurement could be partly attributed to the exfoliation of the loaded catalysts on the glassy carbon electrode (Figure 4c, inset). In order to alleviate the issue of this exfoliation, catalyst ink could be dropped dried onto a 0.8 cm × 0.8 cm Ni foam and then used as the working electrode to conduct chronoamperometric stability measurement. The two flat lines in Figure 4d further demonstrate that the Co_3O_4-B OER catalysts have an excellent electrochemical durability even at a high current density of 50 mA cm^{-2} for 5 h. Remarkably, the polarization curve of Co_3O_4-B after 10 h chronoamperometric test is basically identical with the initial one (Figure 4d, inset), which confirms again the excellent electrochemical durability of Co_3O_4-B studied in this work.

To elucidate the origins of all these catalytic performance enhancement, it is of great importance to explore the change in electrochemical active sites of the samples. In general, the number of such active sites is directly proportional to the electrochemical surface area (ECSA), and the electrochemical surface area (ECSA) is linearly proportional to the double-layer capacitance (C_{dl}) of the electrocatalysts. Therefore, the C_{dl} is often used to represent the corresponding ECSA. By plotting

DOI: 10.1021/acsami.7b18208
ACS Appl. Mater. Interfaces 2018, 10, 7079−7086

the $\Delta j = (j_a - j_c)$ at 0.225 V vs SCE against the scan rate, the linear slope that is twice the double-layer capacitance (C_{dl}) can be obtained as shown in Figure S4. It is also noted that there is a 10-fold increase in C_{dl} from 2.14 mF cm^{-2} for Co_3O_4 to 22.13 mF cm^{-2} for Co_3O_4-B (Figure 5a), demonstrating that more active sites have been generated via $NaBH_4$ reduction process. For a better understanding to the superior OER performance of Co_3O_4-B catalysts, electrical impedance spectroscopy (EIS) is utilized to illustrate the electrochemical kinetics of catalytic processes involved. The fitted Nyquist plots in Figure 5b reveal the charge-transfer resistance (R_{ct} = 38.08 ohm) of porous Co_3O_4-B nanosheets being about 30-fold lower than that of unreduced porous Co_3O_4 nanosheets (R_{ct} = 1256 ohm), further designating that the Co_3O_4-B catalysts possess a much faster charge-transfer characteristic than that of unreduced Co_3O_4 catalysts during the OER process.

For sheetlike nanomaterials, their catalytic activity is always highly depended on the exposed crystal facets, in which the corresponding adsorption/desorption characteristics of reactants, intermediates, and products are largely influenced.[40,41] Generally, high-index facets exposed surface could provide more catalytically favorable surface atomic structures, such as the high density of atomic steps, ledges, and kinks.[25,42,43] In this work, we have prepared different facets (e.g., {110} and {111}) exposed Co_3O_4 nanosheets (see synthetic methods in Supporting Information),[44] in which all of them have been reduced via the same $NaBH_4$ treatment. As depicted in HRTEM images and corresponding FFT patterns in Figure 6,

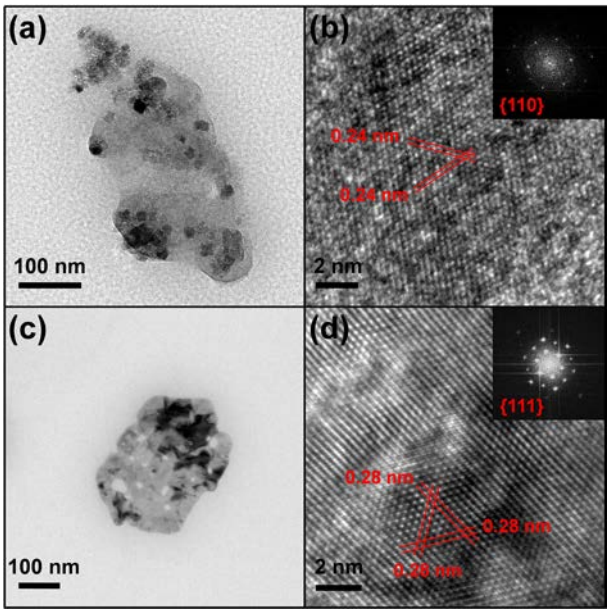

Figure 6. Typical TEM and HRTEM images of (a, b) {110} facets exposed Co_3O_4 nanosheets after 0.5 M $NaBH_4$ solution treatments and (c, d) {111} facets exposed Co_3O_4 nanosheets after 0.5 M $NaBH_4$ solution treatments. Insets are the corresponding FFT patterns.

the morphology of Co_3O_4 nanosheets is well preserved with the same exposed facets after $NaBH_4$ reduction process. As expected, more oxygen vacancies are formed which can be seen from the comparison of O 1s XPS profiles in Figure S5, while the integrated intensity of O_{II} peaks is increased in both samples. The comparison of electrochemical measurement among three different exposure facets of {110}, {111}, and {112} is also displayed in Figure 7. Based on the LSV curves as shown in Figure 7a, the {112} high-index facets exposed Co_3O_4-B nanosheets exhibit the higher OER activity (318 mV) than the counterparts of {110} and {111} exposed facets (320 and 339 mV) at a current density of 10 mA cm^{-2}. Even though the differences in overpotential are not significant, a steepest uptrend of {112} facets exposed Co_3O_4-B illustrates a robust increase in its current density as the potential increases, which is consistent with the corresponding Tafel plots observed in Figure 7b. In order to obtain reliable results, we also adopted BET method to normalize the electrocatalytic activities. Figure S6 shows that the specific surface area of {110} and {111} faceted samples are 49.31 and 33.34 cm^2 g^{-1}, respectively. Similarly, {112} and {110} facets exposed Co_3O_4-B as well performed better than the one of {111} as shown in Figure S7. The better performance could be ascribed to the higher ratio of Co^{2+}/Co^{3+} for the {112} facets, which can further provides more active sites for water oxidation.[26,38] The Tafel values of {110}, {111}, and {112} facets exposed Co_3O_4-B nanosheets are determined to be 66.0, 69.4, and 57.6 mV dec^{-1}, respectively. Also, the current density variation plotted against scan rate can further enable us to estimate the C_{dl} of these three kinds of Co_3O_4-B nanosheets with different exposed facets and elucidate the origin of difference in OER activities in terms of ECSA (in Figure S8 and Figure 7c). The C_{dl} values of 8.42 and 5.53 mF cm^{-2} are calculated for the {110} and {111} exposed samples, which are much smaller than that of {112} one with C_{dl} value of 22.13 mF cm^{-2}. This finding indicates clear that the {112} facets exposed Co_3O_4-B has more electrochemical active sites for OER process as compared with the other two counterparts. Likewise, the comparison of electrochemical kinetics has been conducted using EIS measurement. Apparently, the {111} facets exposed Co_3O_4-B nanosheets feature a much higher charge-transfer resistance of 150.50 ohm than that of the {110} samples (66.77 ohm) and {112} samples (38.08 ohm) as shown in Figure 7d, manifesting a much lower electron transfer rate here during the electrochemical process. Therefore, all these above results have clearly indicated that our high-index faceted porous Co_3O_4-B nanosheets can be advantageously utilized as electrocatalyst materials to drive OER at a significant rate at ultralow overpotentials.

4. CONCLUSION

In summary, {112} high-index faceted porous Co_3O_4 nanosheets with high oxygen vacancy content have been successfully prepared via a facile method followed by $NaBH_4$ solution treatment. These novel structured Co_3O_4 nanosheets exhibit the superior electrocatalytic activity and stability for OER. At overpotentials of 318 and 436 mV, the OER catalysts can deliver current densities of 10 and 800 mA cm^{-2} with an impressively low Tafel slope of 57.6 mV dec^{-1}, which shows the best OER performance among most recently reported cobalt oxide-based materials. These excellent OER performance parameters are mostly attributed to the ultrathin porous structure, {112} high-index exposed facets with higher density of Co^{2+} active sites and oxygen vacancies on surface, which can significantly enhance the charge transfer rate and increase the number of active sites during the OER process. As a result, all these findings can not only demonstrate the technological potency of the uniquely configured Co_3O_4 nanosheets for efficient water oxidation but also provide further insights into the preparation of cost-effective and high-performance transition-metal oxide-based catalysts for electrochemical applications.

DOI: 10.1021/acsami.7b18208
ACS Appl. Mater. Interfaces 2018, 10, 7079−7086

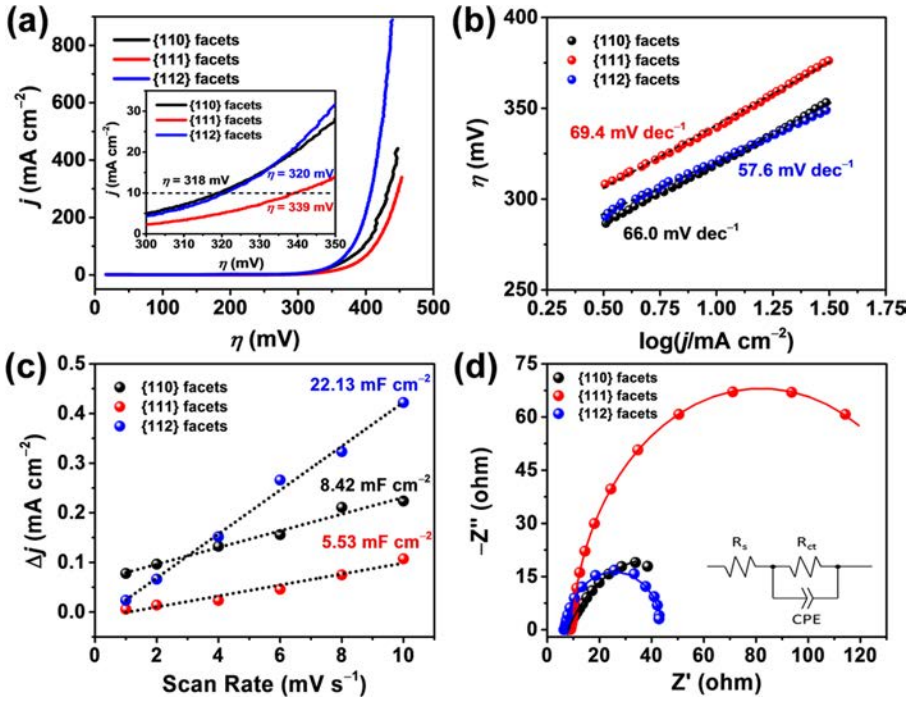

Figure 7. Electrochemical activity comparison of different facets exposed Co_3O_4 nanosheets (a) LSV curves with a scan rate of 5 mV s^{-1} in 1 M KOH solution; inset is the enlarged version with an overpotential window from 300 to 350 mV. (b) Tafel plots and corresponding linear fittings. (c) Differences in current density variation at a potential of 0.225 V (vs SCE) plotted against scan rate fitted to a linear regression, enabling the estimation of C_{dl}. (d) Nyquist plots obtained from the electrochemical impedance spectroscopy measurements at 1.55 V (vs RHE) with a frequency range of 0.01 to 3×10^5 Hz.

■ ASSOCIATED CONTENT

Supporting Information

The Supporting Information is available free of charge on the ACS Publications website at DOI: 10.1021/acsami.7b18208.

Preparation of {110} and {111} facets exposed Co_3O_4 nanosheets with surface oxygen vacancies, XRD pattern, TEM and HRTEM images, XPS profiles, nitrogen adsorption and desorption isotherms and pore size distributions, LSV curves normalized by the BET method, CV curves with different scan rates, comparison table of OER process (PDF)

OER process facilitated by the Co_3O_4-B electrocatalysts (AVI)

■ AUTHOR INFORMATION

Corresponding Author

*E-mail: johnnyho@cityu.edu.hk (J.C.H.)

ORCID

Renjie Wei: 0000-0002-0459-7196

Johnny C. Ho: 0000-0003-3000-8794

Notes

The authors declare no competing financial interest.

■ ACKNOWLEDGMENTS

This work is financially supported by the National Natural Science Foundation of China (Grant 51672229), the Environment and Conservation Fund of Hong Kong SAR, China (ECF 2016-85), the General Research Fund (CityU 11213115) and the Theme-based Research Scheme (T42-103/16-N) of the Research Grants Council of Hong Kong SAR, China, and the Science Technology and Innovation Committee of Shenzhen Municipality (Grant JCYJ20160229165240684), and a grant from the Shenzhen Research Institute, City University of Hong Kong.

■ REFERENCES

(1) Hunter, B. M.; Gray, H. B.; Müller, A. M. Earth-Abundant Heterogeneous Water Oxidation Catalysts. *Chem. Rev.* **2016**, *116*, 14120−14136.

(2) Jiao, Y.; Zheng, Y.; Jaroniec, M.; Qiao, S. Z. Design of Electrocatalysts for Oxygen- and Hydrogen-Involving Energy Conversion Reactions. *Chem. Soc. Rev.* **2015**, *44*, 2060−2086.

(3) Cheng, G.; Kou, T.; Zhang, J.; Si, C.; Gao, H.; Zhang, Z. O_2^{2-}/O-Functionalized Oxygen-Deficient Co_3O_4 Nanorods as High Performance Supercapacitor Electrodes and Electrocatalysts towards Water Splitting. *Nano Energy* **2017**, *38*, 155−166.

(4) Man, I. C.; Su, H. Y.; Calle-Vallejo, F.; Hansen, H. A.; Martínez, J. I.; Inoglu, N. G.; Kitchin, J.; Jaramillo, T. F.; Nørskov, J. K.; Rossmeisl, J. Universality in Oxygen Evolution Electrocatalysis on Oxide Surfaces. *ChemCatChem* **2011**, *3*, 1159−1165.

(5) Cao, R.; Lee, J.-S.; Liu, M.; Cho, J. Recent Progress in Non-Precious Catalysts for Metal-Air Batteries. *Adv. Energy Mater.* **2012**, *2*, 816−829.

(6) Ledendecker, M.; Clavel, G.; Antonietti, M.; Shalom, M. Highly Porous Materials as Tunable Electrocatalysts for the Hydrogen and Oxygen Evolution Reaction. *Adv. Funct. Mater.* **2015**, *25*, 393−399.

(7) Dong, G.; Fang, M.; Zhang, J.; Wei, R.; Shu, L.; Liang, X.; Yip, S.; Wang, F.; Guan, L.; Zheng, Z.; Ho, J. C. In Situ Formation of Highly Active Ni−Fe Based Oxygen-Evolving Electrocatalysts via Simple Reactive Dip-Coating. *J. Mater. Chem. A* **2017**, *5*, 11009−11015.

(8) Deng, X.; Tüysüz, H. Cobalt-Oxide-Based Materials as Water Oxidation Catalyst: Recent Progress and Challenges. *ACS Catal.* **2014**, *4*, 3701−3714.

(9) Osgood, H.; Devaguptapu, S. V.; Xu, H.; Cho, J.; Wu, G. Transition Metal (Fe, Co, Ni, and Mn) Oxides for Oxygen Reduction

and Evolution Bifunctional Catalysts in Alkaline Media. *Nano Today* **2016**, *11*, 601−625.
(10) Zhou, X.; Shen, X.; Xia, Z.; Zhang, Z.; Li, J.; Ma, Y.; Qu, Y. Hollow Fluffy Co_3O_4 Cages as Efficient Electroactive Materials for Supercapacitors and Oxygen Evolution Reaction. *ACS Appl. Mater. Interfaces* **2015**, *7*, 20322−20331.
(11) Yang, J.; Zhou, T.; Zhu, R.; Chen, X.; Guo, Z.; Fan, J.; Liu, H. K.; Zhang, W.-X. Highly Ordered Dual Porosity Mesoporous Cobalt Oxide for Sodium-Ion Batteries. *Adv. Mater. Interfaces* **2016**, *3*, 1500464.
(12) Wang, H.; Zhou, T.; Li, D.; Gao, H.; Gao, G.; Du, A.; Liu, H.; Guo, Z. Ultrathin Cobaltosic Oxide Nanosheets as an Effective Sulfur Encapsulation Matrix with Strong Affinity Toward Polysulfides. *ACS Appl. Mater. Interfaces* **2017**, *9*, 4320−4325.
(13) Yan, X.; Tian, L.; He, M.; Chen, X. Three-Dimensional Crystalline/Amorphous Co/Co_3O_4 Core/Shell Nanosheets as Efficient Electrocatalysts for the Hydrogen Evolution Reaction. *Nano Lett.* **2015**, *15*, 6015−6021.
(14) Aijaz, A.; Masa, J.; Rösler, C.; Xia, W.; Weide, P.; Botz, A. J. R.; Fischer, R. A.; Schuhmann, W.; Muhler, M. $Co@Co_3O_4$ Encapsulated in Carbon Nanotube-Grafted Nitrogen-Doped Carbon Polyhedra as an Advanced Bifunctional Oxygen Electrode. *Angew. Chem., Int. Ed.* **2016**, *55*, 4087−4091.
(15) Hang, L.; Sun, Y.; Men, D.; Liu, S.; Zhao, Q.; Cai, W.; Li, Y. Hierarchical Micro/nanostructured C Doped Co/Co_3O_4 Hollow Spheres Derived from $PS@Co(OH)_2$ for the Oxygen Evolution Reaction. *J. Mater. Chem. A* **2017**, *5*, 11163−11170.
(16) Luo, W.; Wang, Y.; Wang, L.; Jiang, W.; Chou, S.-L.; Dou, S. X.; Liu, H. K.; Yang, J. Silicon/Mesoporous Carbon/Crystalline TiO_2 Nanoparticles for Highly Stable Lithium Storage. *ACS Nano* **2016**, *10*, 10524−10532.
(17) Liang, Y.; Li, Y.; Wang, H.; Zhou, J.; Wang, J.; Regier, T.; Dai, H. Co_3O_4 Nanocrystals on Graphene as a Synergistic Catalyst for Oxygen Reduction Reaction. *Nat. Mater.* **2011**, *10*, 780−786.
(18) He, B.; Chen, X.; Lu, J.; Yao, S.; Wei, J.; Zhao, Q.; Jing, D.; Huang, X.; Wang, T. One-Pot Synthesized Co/Co_3O_4 -N-Graphene Composite as Electrocatalyst for Oxygen Reduction Reaction and Oxygen Evolution Reaction. *Electroanalysis* **2016**, *28*, 2435−2443.
(19) Wu, Z.; Sun, L.-P.; Yang, M.; Huo, L.-H.; Zhao, H.; Grenier, J.-C. Facile Synthesis and Excellent Electrochemical Performance of Reduced Graphene oxide−Co_3O_4 Yolk-Shell Nanocages as a Catalyst for Oxygen Evolution Reaction. *J. Mater. Chem. A* **2016**, *4*, 13534−13542.
(20) Liu, Y.; Zhou, T.; Zheng, Y.; He, Z.; Xiao, C.; Pang, W. K.; Tong, W.; Zou, Y.; Pan, B.; Guo, Z.; Xie, Y. Local Electric Field Facilitates High-Performance Li-Ion Batteries. *ACS Nano* **2017**, *11*, 8519−8526.
(21) Wang, Y.; Zhou, T.; Jiang, K.; Da, P.; Peng, Z.; Tang, J.; Kong, B.; Cai, W.-B.; Yang, Z.; Zheng, G. Reduced Mesoporous Co_3O_4 Nanowires as Efficient Water Oxidation Electrocatalysts and Supercapacitor Electrodes. *Adv. Energy Mater.* **2014**, *4*, 1400696.
(22) Xu, L.; Jiang, Q.; Xiao, Z.; Li, X.; Huo, J.; Wang, S.; Dai, L. Plasma-Engraved Co_3O_4 Nanosheets with Oxygen Vacancies and High Surface Area for the Oxygen Evolution Reaction. *Angew. Chem., Int. Ed.* **2016**, *55*, 5277−5281.
(23) Xu, L.; Wang, Z.; Wang, J.; Xiao, Z.; Huang, X.; Liu, Z.; Wang, S. N-Doped Nanoporous Co_3O_4 Nanosheets with Oxygen Vacancies as Oxygen Evolving Electrocatalysts. *Nanotechnology* **2017**, *28*, 165402.
(24) Stoerzinger, K. A.; Qiao, L.; Biegalski, M. D.; Shao-Horn, Y. Orientation-Dependent Oxygen Evolution Activities of Rutile IrO_2 and RuO_2. *J. Phys. Chem. Lett.* **2014**, *5*, 1636−1641.
(25) Feng, L. L.; Yu, G.; Wu, Y.; Li, G. D.; Li, H.; Sun, Y.; Asefa, T.; Chen, W.; Zou, X. High-Index Faceted Ni_3S_2 Nanosheet Arrays as Highly Active and Ultrastable Electrocatalysts for Water Splitting. *J. Am. Chem. Soc.* **2015**, *137*, 14023−14026.
(26) Liu, L.; Jiang, Z.; Fang, L.; Xu, H.; Zhang, H.; Gu, X.; Wang, Y. Probing the Crystal Plane Effect of Co_3O_4 for Enhanced Electrocatalytic Performance toward Efficient Overall Water Splitting. *ACS Appl. Mater. Interfaces* **2017**, *9*, 27736−27744.
(27) Wei, R.; Zhou, X.; Zhou, T.; Hu, J.; Ho, J. C. Co_3O_4 Nanosheets with In-Plane Pores and Highly Active {112} Exposed Facets for High Performance Lithium Storage. *J. Phys. Chem. C* **2017**, *121*, 19002−19009.
(28) Fang, M.; Dong, G.; Wei, R.; Ho, J. C. Hierarchical Nanostructures: Design for Sustainable Water Splitting. *Adv. Energy Mater.* **2017**, *7*, 1700559.
(29) Yan, Y.; Thia, L.; Xia, B. Y.; Ge, X.; Liu, Z.; Fisher, A.; Wang, X. Construction of Efficient 3D Gas Evolution Electrocatalyst for Hydrogen Evolution: Porous FeP Nanowire Arrays on Graphene Sheets. *Adv. Sci.* **2015**, *2*, 1500120.
(30) Wei, R.; Hu, J.; Zhou, T.; Zhou, X.; Liu, J.; Li, J. Ultrathin SnS_2 Nanosheets with Exposed {001} Facets and Enhanced Photocatalytic Properties. *Acta Mater.* **2014**, *66*, 163−171.
(31) Han, L.; Dong, S.; Wang, E. Transition-Metal (Co, Ni, and Fe)-Based Electrocatalysts for the Water Oxidation Reaction. *Adv. Mater.* **2016**, *28* (42), 9266−9291.
(32) Huang, J.; Chen, J.; Yao, T.; He, J.; Jiang, S.; Sun, Z.; Liu, Q.; Cheng, W.; Hu, F.; Jiang, Y.; Pan, Z.; Wei, S. CoOOH Nanosheets with High Mass Activity for Water Oxidation. *Angew. Chem., Int. Ed.* **2015**, *54*, 8722−8727.
(33) Sun, Y. F.; Gao, S.; Lei, F. C.; Liu, J. W.; Liang, L.; Xie, Y. Atomically-Thin Non-Layered Cobalt Oxide Porous Sheets for Highly Efficient Oxygen-Evolving Electrocatalysts. *Chem. Sci.* **2014**, *5*, 3976−3982.
(34) Huang, H.; Zhu, W.; Tao, X.; Xia, Y.; Yu, Z.; Fang, J.; Gan, Y.; Zhang, W. Nanocrystal-Constructed Mesoporous Single-Crystalline Co_3O_4 Nanobelts with Superior Rate Capability for Advanced Lithium-Ion Batteries. *ACS Appl. Mater. Interfaces* **2012**, *4*, 5974−5980.
(35) Jiang, J.; Zhang, A.; Li, L.; Ai, L. Nickel-Cobalt Layered Double Hydroxide Nanosheets as High-Performance Electrocatalyst for Oxygen Evolution Reaction. *J. Power Sources* **2015**, *278*, 445−451.
(36) Petitto, S. C.; Marsh, E. M.; Carson, G. A.; Langell, M. A. Cobalt Oxide Surface Chemistry: The Interaction of CoO(100), Co_3O_4(110) and Co_3O_4(111) with Oxygen and Water. *J. Mol. Catal. A: Chem.* **2008**, *281*, 49−58.
(37) Yang, Z. K.; Lin, L.; Xu, A. 2D Nanoporous Fe−N/C Nanosheets as Highly Efficient Non-Platinum Electrocatalysts for Oxygen Reduction Reaction in Zn-Air Battery. *Small* **2016**, *12*, 5710−5719.
(38) Wang, H.-Y.; Hung, S.-F.; Chen, H.-Y.; Chan, T.-S.; Chen, H. M.; Liu, B. In Operando Identification of Geometrical-Site-Dependent Water Oxidation Activity of Spinel Co_3O_4. *J. Am. Chem. Soc.* **2016**, *138*, 36−39.
(39) Bao, J.; Zhang, X.; Fan, B.; Zhang, J.; Zhou, M.; Yang, W.; Hu, X.; Wang, H.; Pan, B.; Xie, Y. Ultrathin Spinel-Structured Nanosheets Rich in Oxygen Deficiencies for Enhanced Electrocatalytic Water Oxidation. *Angew. Chem., Int. Ed.* **2015**, *54*, 7399−7404.
(40) Xie, X.; Li, Y.; Liu, Z.-Q.; Haruta, M.; Shen, W. Low-Temperature Oxidation of CO Catalysed by Co_3O_4 Nanorods. *Nature* **2009**, *458*, 746−749.
(41) Kuo, C.-H.; Mosa, I. M.; Thanneeru, S.; Sharma, V.; Zhang, L.; Biswas, S.; Aindow, M.; Pamir Alpay, S.; Rusling, J. F.; Suib, S. L.; He, J. Facet-Dependent Catalytic Activity of MnO Electrocatalysts for Oxygen Reduction and Oxygen Evolution Reactions. *Chem. Commun.* **2015**, *51*, 5951−5954.
(42) Yin, J.; Yu, Z.; Gao, F.; Wang, J.; Pang, H.; Lu, Q. Low-Symmetry Iron Oxide Nanocrystals Bound by High-Index Facets. *Angew. Chem.* **2010**, *122*, 6472−6476.
(43) Quan, Z.; Wang, Y.; Fang, J. High-Index Faceted Noble Metal Nanocrystals. *Acc. Chem. Res.* **2013**, *46*, 191−202.
(44) Su, D.; Dou, S.; Wang, G. Single Crystalline Co_3O_4 Nanocrystals Exposed with Different Crystal Planes for Li-O_2 Batteries. *Sci. Rep.* **2015**, *4*, 5767.

DOI: 10.1021/acsami.7b18208
ACS Appl. Mater. Interfaces 2018, 10, 7079−7086